JACS
JOURNAL OF THE AMERICAN CHEMICAL SOCIETY
Article
pubs.acs.org/JACS

Self-Exfoliated Guanidinium-Based Ionic Covalent Organic Nanosheets (iCONs)

Shouvik Mitra,[†,▽] Sharath Kandambeth,[†,∥,▽] Bishnu P. Biswal,[†,∥,▽] Abdul Khayum M.,[†,∥] Chandan K. Choudhury,[†,∥] Mihir Mehta,[‡,∥] Gagandeep Kaur,[⊥] Subhrashis Banerjee,[†,∥] Asmita Prabhune,[‡,∥] Sandeep Verma,[⊥] Sudip Roy,[†] Ulhas K. Kharul,[§,∥] and Rahul Banerjee*[,†,∥]

[†]Physical/Materials Chemistry Division, [‡]Biochemical Sciences Division, and [§]Polymer Science and Engineering Division, CSIR-National Chemical Laboratory, Pune 411008, India

[∥]Academy of Scientific and Innovative Research (AcSIR), New Delhi 110020, India

[⊥]Department of Chemistry, Indian Institute of Technology, Kanpur 208016, India

Supporting Information

ABSTRACT: Covalent organic nanosheets (CONs) have emerged as functional two-dimensional materials for versatile applications. Although $\pi-\pi$ stacking between layers, hydrolytic instability, possible restacking prevents their exfoliation on to few thin layered CONs from crystalline porous polymers. We anticipated rational designing of a structure by intrinsic ionic linker could be the solution to produce self-exfoliated CONs without external stimuli. In an attempt to address this issue, we have synthesized three self-exfoliated guanidinium halide based ionic covalent organic nanosheets (iCONs) with antimicrobial property. Self-exfoliation phenomenon has been supported by molecular dynamics (MD) simulation as well. Intrinsic ionic guanidinium unit plays the pivotal role for both self-exfoliation and antibacterial property against both Gram-positive and Gram-negative bacteria. Using such iCONs, we have devised a mixed matrix membrane which could be useful for antimicrobial coatings with plausible medical benefits.

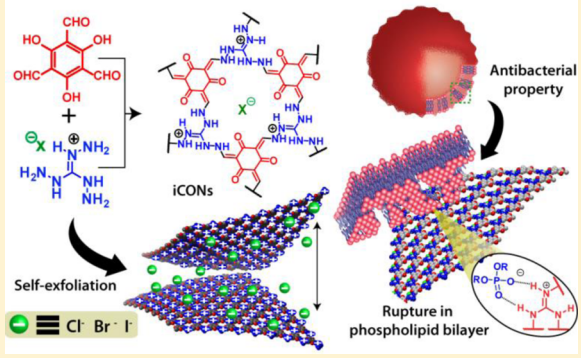

INTRODUCTION

Covalent organic nanosheets (CONs) are two-dimensional (2D) materials constructed by symmetrically arranged organic linkers, along two dimension, via strong covalent bonds.[1] In recent years, researchers have made considerable efforts to synthesize monolayer or few layered CONs, which could emerge as a porous functional material with a plethora of applications owing to their easy and predesignable functionalization opportunity.[1,2] On this line, few layered CONs have been synthesized from 2D crystalline porous polymers (CPPs) often known as covalent organic frameworks (COFs)[3] and covalent triazine frameworks (CTFs),[4] using conventional exfoliation techniques such as ultrasonication[1c] and mechanical delamination.[1a,b,d] However, the major reasons that prevent the formation of monolayer or few layered CONs by these methods include (i) strong $\pi-\pi$ stacking between the layers,[1−4] (ii) hydrolytic instability for most of the CPPs,[5] (iii) possible restacking,[6] and most importantly, (iv) challenging synthetic procedures to obtain the exfoliated nanosheets.[1e,7] However, these shortcomings could be surpassed easily by rational design of chemically stable CONs with inbuilt ionic character to induce self-exfoliation. Moreover, if the ionic building block itself possesses biological significance, the synthesized CONs could be directly used for biomedical applications without further post synthetic modifications. Nevertheless, the self-exfoliation of 2D CPPs and exploring its biological significance in a single domain is unprecedented and thus remains a daunting task. In the same pursuit, we have introduced the concept of rational design to self-exfoliate guanidinium halide based porous ionic covalent organic nanosheets (iCONs) for antimicrobial applications. Positively charged guanidinium units result in interlayer repulsion to self-exfoliate into few layered iCONs. These iCONs showed permanent porosity, chemical stability and potent antimicrobial property against both Gram-positive (*Staphylococcus aureus*) and Gram-negative (*Escherichia coli*) bacteria. Although substituted guanidinium-based conventional polymeric materials are known to demonstrate antimicrobial property;[8] but the solubility of guanidinium-based materials limits their usage in heterogeneous water resistant antimicrobial coatings. Hence, the insolubility of iCONs with antimicrobial property could be the key solution in devising antibacterial coatings useful in biomedical sectors. To validate this conception, we have strategically fabricated iCONs@Polysulfone (PSF) mixed matrix membrane for antimicrobial coatings.

Received: December 29, 2015
Published: February 11, 2016

DOI: 10.1021/jacs.5b13533
J. Am. Chem. Soc. 2016, 138, 2823−2828

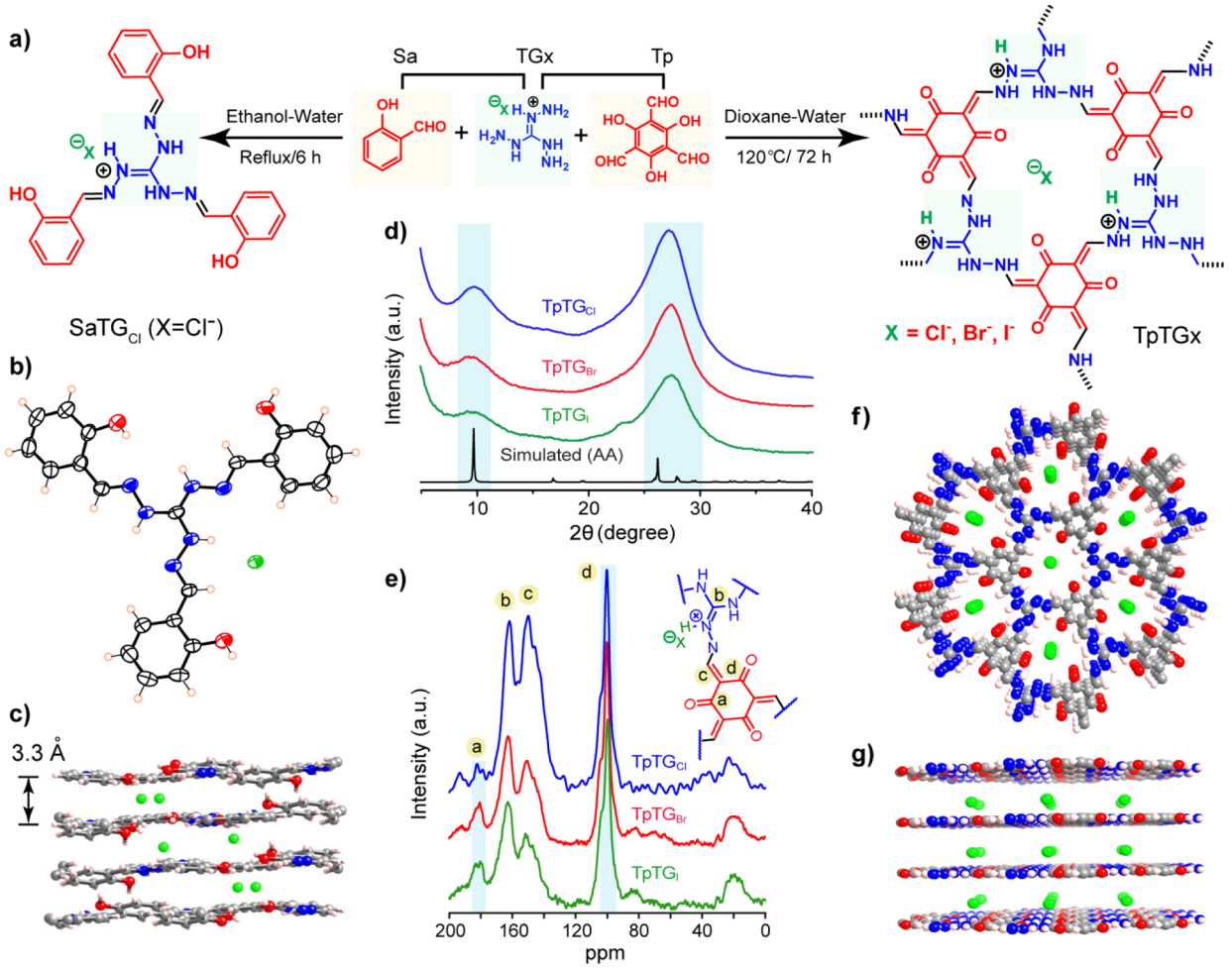

Figure 1. (a) Synthetic scheme of $TpTG_{Cl}$ monomer ($SaTG_{Cl}$) (left) and of iCONs ($TpTG_X$) (right); where X = Cl^-, Br^-, I^-. (b) ORTEP diagram of $SaTG_{Cl}$ at 50% probability ellipsoid level. (c) Stacking model of $SaTG_{Cl}$ showing sandwiched anions between the layers (side view). (d) Comparison of PXRD patterns of the three iCONs. (e) ^{13}C CP MAS solid-state NMR of iCONs. (f) Modeling of $TpTG_{Cl}$ in eclipsed mode (top view). (g) Stacking model showing individual layers (side view).

EXPERIMENTAL SECTION

Three of the iCONs ($TpTG_{Cl}$, $TpTG_{Br}$, and $TpTG_I$) were synthesized via Schiff base condensation reaction between 0.2 mmol 1,3,5-triformylphloroglucinol (Tp) (42 mg) and 0.2 mmol amines (TG_X) (TG_{Cl}, 28 mg or TG_{Br}, 37 mg or TG_I, 47.4 mg) in a sealed Pyrex tube using dioxane/water in the ratio 2:0.6 mL. The reaction mixtures were charged into Pyrex tube and sonicated for 20 min. The mixtures were degassed under liquid N_2 (77K) by freeze–pump–thaw cycles for three times, and the Pyrex tube was then vacuum sealed. The reaction mixtures were allowed to attend room temperature and then kept at 120 °C for 3 days. $TpTG_{Cl}$, $TpTG_{Br}$, and $TpTG_I$ were obtained as a brown colored precipitate. The product was washed thoroughly with DMAc, water, and acetone, respectively, and dried at 90 °C for overnight to obtain ~70% isolated yield.

To obtain detail insights into self-exfoliation of iCONs in the presence of water molecules, we performed all atom molecular dynamics (MD) simulations (detailed in section S-8 in the Supporting Information).The synthesized iCONs were used for antibacterial studies using three different concentrations (100, 200, and 500 $\mu g\ mL^{-1}$). They were dispersed in autoclaved deionized water and allowed to incubate with bacterial strains *Staphylococcus aureus* and *Escherichia coli* for about 4 h. The resulting mixture was plated in Petri plates containing solidified potato dextrose agar media. The Petri plates were incubated at 37 °C for 24 h, and the resulting CFU counts were measured visually. Morphological study of control and treated bacterial samples were carried out by SEM and TEM. Detailed experimental procedures are provided in section S-10 in the Supporting Information. We further fabricated iCONs mixed matrix membrane using PSF on porous nonwoven support fabrics (3329). $TpTG_{Cl}$ (5% by wt of PSF) was added to the PSF solution in DMF, stirred well for another 6 h, and degassed for 3 min to remove the trapped gases. $TpTG_{Cl}$@PSF membranes were prepared using Sheen Automatic Film Applicator-1132 at 25 °C and exposed in air for 15 s prior to dipping in nonsolvent (water) bath. The knife movement was set to 10 cm s^{-1} transverse speed with a gap of 250 μm. The total thickness of the supported membrane was ~100 μm. These membranes were washed with distilled water and stored in aqueous formalin (0.5%) solution. Antibacterial activity of iCONs membrane was evaluated by the growth of bacteria on to it (detailed in section S-11 in the Supporting Information).

RESULTS AND DISCUSSION

In order to incorporate guanidinium units within a stable iCONs framework, we have synthesized triaminoguanidinium halide (TG_{Cl}, TG_{Br}, and TG_I) which assumes a C_3 symmetric planner structure (sections S-2 and S-3, Supporting Information).[9] These C_3 symmetric amines resulted into three 2D iCONs ($TpTG_{Cl}$, $TpTG_{Br}$, and $TpTG_I$) when reacted with C_3 symmetric Tp (Figure 1a). PXRD patterns of these three iCONs revealed low crystallinity with the first broad peak at 2θ = ~ 9.7° which corresponds to100 plane (Figure 1d). The major broad peak at 2θ = ~ 27.3° signified poor π–π stacking between the vertically stacked layers (Figure 1d). In order to get precise

DOI: 10.1021/jacs.5b13533
J. Am. Chem. Soc. 2016, 138, 2823–2828

structural insights, monomeric unit of $TpTG_{Cl}$ was synthesized and crystallized (Figure 1a).[10] The single crystal structure of the monomer showed the presence of Cl^- anion sandwiched between two monomer units (~3.3 Å), which remain hydrogen bonded [N−H···Cl^-; D = 3.29 Å, d = 2.57 Å, θ = 141.8°] with the guanidinium nitrogen and hydroxyl group of salicylaldehyde (Figure 1b).[11] Presence of this loosely bound chloride ions and intrinsic positive charge of guanidinium units (Figure 1c) disturb the $\pi-\pi$ stacking interactions among the layers in the extended iCONs structure, which we believe is the reason for their low crystallinity. Based on the monomer structure, all three iCONs ($TpTG_{Cl}$, $TpTG_{Br}$, and $TpTG_I$) were modeled in possible 2D eclipsed and staggered structure (Figure 1f, Section S4 ESI). The PXRD pattern of fully eclipsed AA structure matched well with that of experimentally observed PXRD (Figures S6−S11). Although the monomeric units were planner, but ionic layers with sandwiched halide ions in between them created an extremely weak stacking (Figure 1g). This motivated us to believe that the as-synthesized polymers would intrinsically self-exfoliate to covalent organic nanosheets.

FTIR spectra of iCONs revealed characteristic C═C stretching frequency at 1597 cm^{-1} and C−N stretching frequency at 1291 cm^{-1},[1d,12] while characteristic carbonyl and primary amine stretching frequency of the precursors was absent (Figure S12). Similarly, ^{13}C CP-MAS solid-state NMR spectroscopy of $TpTG_X$ showed a very sharp peak at 100.1 ppm which signified the exocyclic C═C carbon[12] adjacent to the C═O carbon (Figure 1e). Signal representing deshielded C═C carbon attached to the N was obtained at 150 ppm. Carbon signal of guanidinium C═N appeared at ~162 ppm, and a small keto (−C═O) carbon signal was noted in between 180 and 182 ppm.[1d,12] The sharp exocyclic double bond signal is the strong evidence of irreversible enol to keto tautomerism in iCONs.[12] In addition, TGA profiles of the iCONs demonstrated their thermal stability up to ~225 °C (Figure S14). Permanent porosity of these iCONs was verified using N_2 adsorption isotherms of the activated samples at 77K, where all three iCONs followed Type-II reversible adsorption isotherm. The Brunauer−Emmett−Teller (BET) surface area of $TpTG_{Cl}$, $TpTG_{Br}$, and $TpTG_I$ were found to be 267, 305, and 298 $m^2\ g^{-1}$, respectively (Figure 2a). This lower surface area of iCONs could be a result of poor layer stacking, small pore diameter, and pore blocking by the counteranions. Pore size distributions were calculated on the basis of nonlocal density function theory (NLDFT). Due to the lack of proper channelled pore structure and pore blocking by subsequent counteranions, no sharp pore size distributions were obtained (Figure 2a inset, Figure S15). These were consistent with the previous report where delamination of 2D-CPP layers into CONs resulted in destruction of finite porosity.[1d]

Self-exfoliation of all three iCONs resulted in micrometer to submicrometer sized sheet directly as observed in SEM (Figure S19); meanwhile, EDX analysis signified C, N, O, and corresponding halogens (Cl^-, Br^- and I^-) as major chemical components in $TpTG_{Cl}$, $TpTG_{Br}$, and $TpTG_I$ (Figure S22). TEM images of $TpTG_{Cl}$, $TpTG_{Br}$, and $TpTG_I$ also showed thin transparent sheets and they were marginally rippled (Figures 3a−c and S20). Average d spacing value (~3.7 Å) obtained from TEM analysis was consistent with corresponding PXRD analysis (Figure S23). TEM analysis was well supported by corresponding AFM measurements carried out in the tapping mode. iCONs sheets, with high aspect ratio, showed that their range of height profile was around 2−5 nm (Figures 3d−f and S21). This indicates that the iCONs could be exfoliated into 3−6 layers.[1e,h,7a]

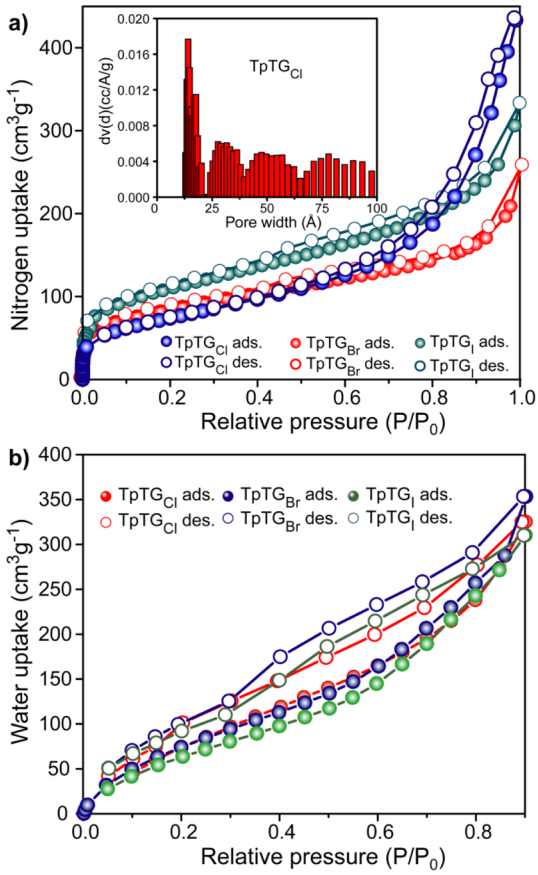

Figure 2. (a) Nitrogen adsorption isotherm and (b) water vapor uptake of $TpTG_{Cl}$, $TpTG_{Br}$, and $TpTG_I$, respectively. Panel (a) inset shows pore size distribution of $TpTG_{Cl}$.

In order to validate self-exfoliation of iCONs, we further used MD simulation studies (section S-8, Supporting Information). Interestingly, in aqueous medium, $TpTG_{Cl}$ layers were found to be exfoliated without any external stimuli, as the average interlayer $\pi-\pi$ stacking distance was increased up to ~5.5−6 Å compared to initial 3.338 Å stacking (Figure 3g and h). Hydration shell surrounding the iCONs and sandwiched halide ions (Cl^- for $TpTG_{Cl}$) further contributed to self-exfoliation mechanism as evident from the simulation studies (Figure S30). Although we have attempted to synthesize CPPs by using neutral ligand (1,2,3-triaminoguanidine), but exfoliated sheet like CONs was not obtained for the same as evident from TEM imaging (Figure S25). Alternatively, we mechanically grinded as-synthesized $TpTG_{Cl}$ and analyzed the PXRD pattern to support the self-exfoliation. No significant alteration in PXRD patterns of as-synthesized and mechanically grinded one was noted, which could be a fare evidence of self-exfoliation phenomenon of iCONs (Figure S18).[1c,d]

These iCONs displayed stable aqueous dispersion for at least 20 days owing to their ionic backbone (Figure S16).[13] A characteristic Tyndall effect was noted signifying stable colloidal suspension during this time (Figure S16).[1d] Hydrophilic environment within the iCONs backbone was reflected in corresponding water adsorption isotherms as 320, 325, and 350 cc g^{-1} water vapor uptake was noted at 0.9P/P_0 (STP), at 298 K for $TpTG_{Cl}$, $TpTG_{Br}$, and $TpTG_I$ respectively (Figure 2b). Chemical stability of these iCONs was ensured in different commonly used solvents such as methanol, acetone, THF, and water for 7 days (Figures S32 and S33). Moreover, these iCONs

DOI: 10.1021/jacs.5b13533
J. Am. Chem. Soc. 2016, 138, 2823−2828

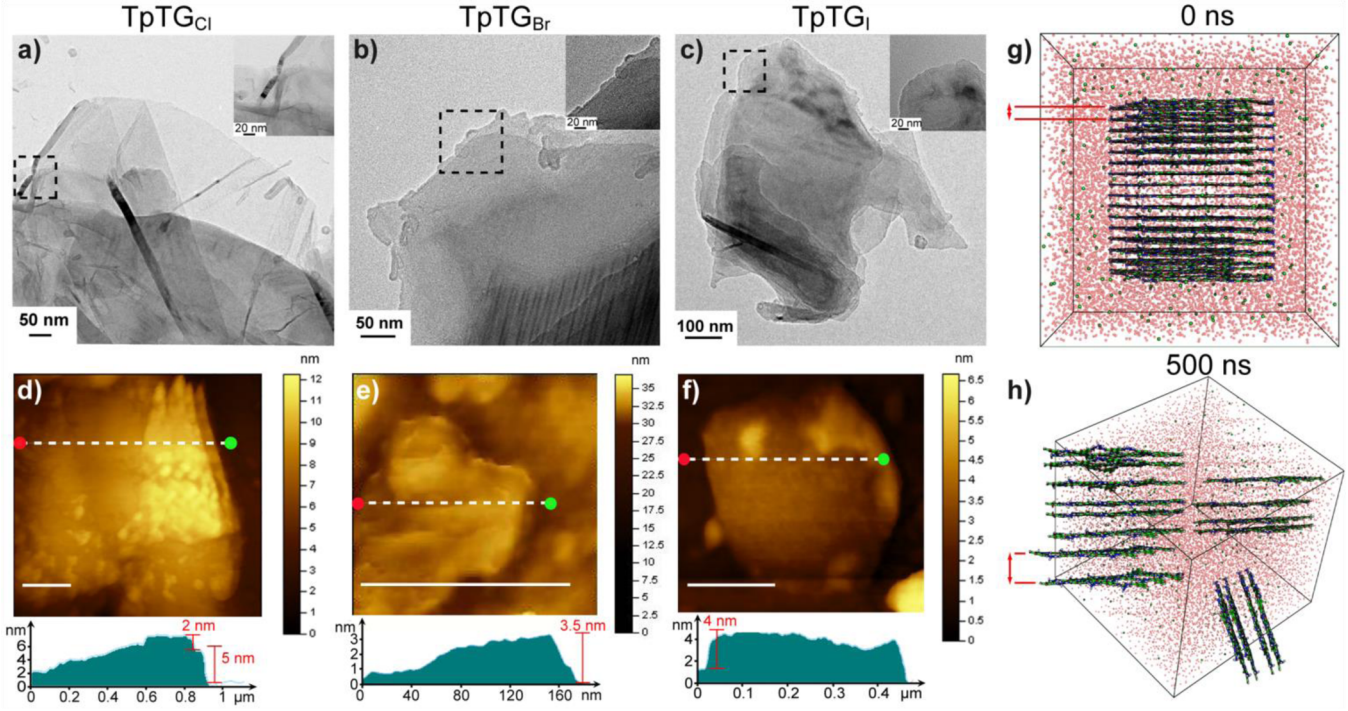

Figure 3. (a–c) TEM images of TpTG$_{Cl}$, TpTG$_{Br}$, and TpTG$_{I}$, respectively (inset shows zoomed in images; scale bar = 20 nm). (d–f) AFM images and height profile of TpTG$_{Cl}$, TpTG$_{Br}$, and TpTG$_{I}$, respectively (AFM scale bars represent 200 nm). MD simulation snapshots of TpTG$_{Cl}$ in aqueous medium demonstrating self-exfoliation: (g) snapshot at initial state (0 ns), (h) snapshot at 500 ns.

showed the stability in 3 N HCl for 7 days, which has been verified by PXRD and FTIR analysis owing to their more stable tautomeric form (Figure S31).[12]

For antibacterial studies, TpTG$_{Cl}$ was selected as the model iCONs. In all TpTG$_{Cl}$ treated sets, colony forming units (CFU) were drastically reduced in a concentration dependent manner for both Gram-positive (*Staphylococcus aureus*) and Gram-negative (*Escherichia coli*) bacteria (Figure S34).[14,15] Therefore, TpTG$_{Cl}$ could be used as antibacterial agent against a broad spectrum of microbial system. Antibacterial activities of TpTG$_{Br}$ and TpTG$_{I}$ were also promising (Figure S35; Table T7, Supporting Information). Hence, it could be concluded that the guanidinium core of the iCONs is responsible for such antimicrobial activity. Meanwhile, morphological studies of control and treated bacterial samples were evaluated by SEM and TEM. Control *S. aureus* was found to be spherical in shape with smooth, continuous, and unbroken cell membranes; while TpTG$_{Cl}$ treated bacterial sample showed rupture in morphology as evident in SEM and TEM imaging (Figure 4a and b). The same observation was noted for *E. coli* where the control sample showed uniform rod shaped morphology and the treated ones illustrated shrunken, twisted rodlike morphology (Figure 4c and d).[14] Planar guanidinium units are known to demonstrate strong binding with the oxoanions of phosphate through two point hydrogen bonding interactions.[16] We speculate, positively charged iCONs could interact with bacterial cells followed by the disruption of negatively charged phospholipid bilayer (Figure 4e).[17] This would result leaching out of the cellular content and subsequently death of the bacteria. Although electrostatic interactions between positively charged guanidinium units and phospholipid bilayers play a pivotal role in antibacterial response of the iCONs, hydrogen bonding interactions between the keto groups of iCONs and phospholipids might have contributed to the antibacterial mechanism as well.[18] Morphological alteration and antibacterial response of iCONs was further verified by live/dead cell imaging study (Figure S36) and cell cycle analysis (Figure S37) of control and treated bacterial cells.

Inspired by antibacterial property and good dispersibility of iCONs we have attempted to device a mixed matrix antimicrobial membrane with PSF and TpTG$_{Cl}$ on a porous support (section S-11, Supporting Information). The resultant membrane (TpTG$_{Cl}$@PSF) was found to be robust, free-standing, stable and highly flexible (Figures 4f and S38). SEM image illustrates the cross section of the fabricated composite membrane (Figure 4g); the presence of iCONs materials was clearly observed as noted by elemental mapping (Figure S39). TpTG$_{Cl}$ was not leached out from the composite membrane materials even after a prolonged period of water treatment conveying good stability as noted by FTIR (Figure S40). It is noteworthy to mention that soluble nature of guanidinium-based compounds in aqueous/organic medium limit their processability for heterogeneous membrane fabrication. Although AgCl-PAF-50 composites have been used for antimicrobial coatings, aqueous instability of such boronic acid based materials could not be ruled out.[15] In contrast, insolubility, aqueous stability, and inherent antimicrobial property of iCONs without further doping paved the way for heterogeneous membrane formulation overcoming the drawbacks. Even iCONs are unlikely to engender oxidative stress, since electrostatic interaction of guanidinium unit is responsible for antibacterial response. Notably, the membrane was hydrophilic in nature with a water contact angle of ~53° at the water–air interface (Figure S38a inset) and allows the permeation of water through it (27 L m^{-2} h^{-1}). Prior to the antimicrobial evaluation of the membrane, the activity of PSF was also checked which showed no significant antimicrobial activity (Figure S42). Antibacterial activity of this TpTG$_{Cl}$@PSF membrane was evaluated by growth of the bacteria on it; in contrast, we took a normal filter paper as a control.[19]

DOI: 10.1021/jacs.5b13533
J. Am. Chem. Soc. 2016, 138, 2823–2828

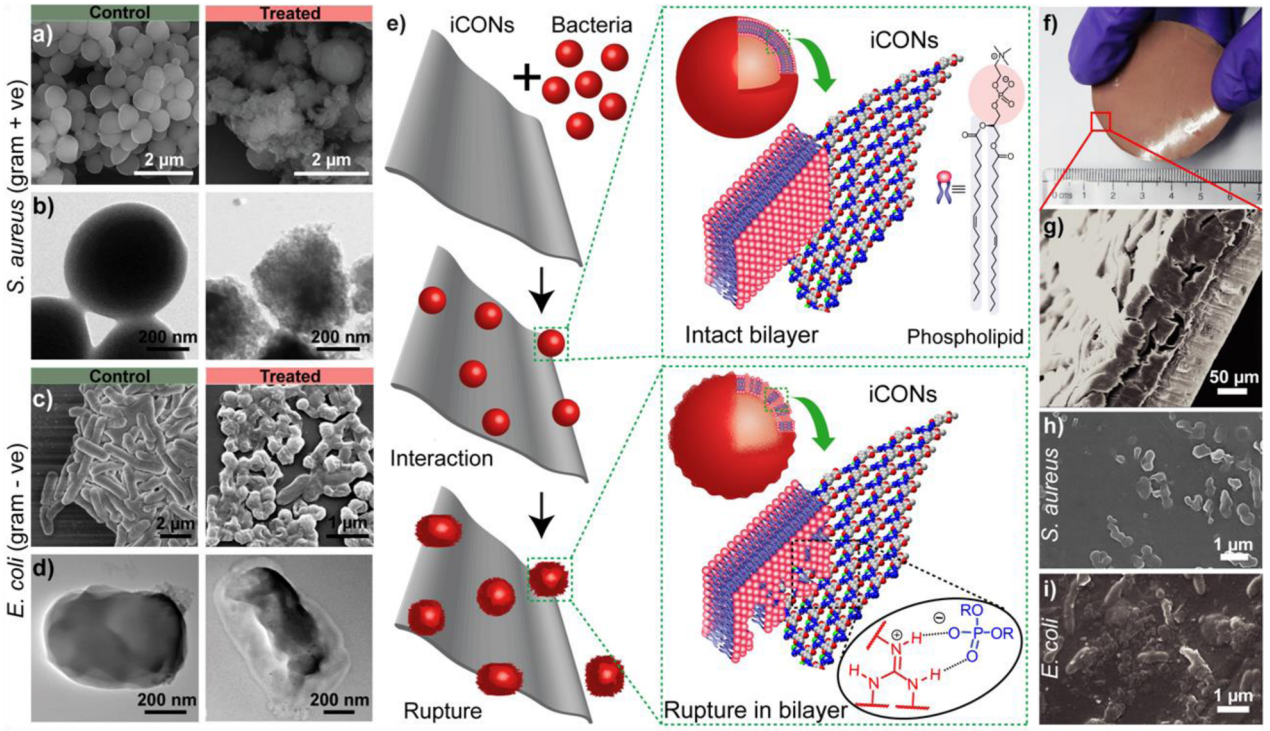

Figure 4. (a) SEM images and (b) TEM images of control and $TpTG_{Cl}$ treated *S. aureus*. (c) SEM images and (d) TEM images of control and $TpTG_{Cl}$ treated *E. coli*. (e) Schematic representation for its mode of action between bacteria and iCONs. (f) Digital image of $TpTG_{Cl}$@PSF mixed matrix membrane. (g) SEM image of the $TpTG_{Cl}$@PSF mixed matrix membrane. Antibacterial property of $TpTG_{Cl}$@PSF mixed matrix membrane by growth of (h) *S. aureus* and (i) *E. coli* on to it.

Interestingly, in filter paper, both the *S. aureus* and *E. coli* retained morphological integrity (Figure S43) which justified no significant antibacterial property. While in $TpTG_{Cl}$@PSF, the membrane showed both shrinking and rupture of the morphology (Figure 4h and i), demonstrating antibacterial property.

CONCLUSION

In summary, we have rationally designed guanidinium-based self-exfoliated antimicrobial porous iCONs. Judiciously designed iCONs were composed of a few thin layers, thanks to the intrinsic charge within the framework backbone and sandwiched anions in between the layers. Since synthesis of thin layered intrinsically ionic 2D materials is challenging, self-exfoliation by incorporation of ionic guanidinium linker could be an alternative to obtain thin layered 2D material without further post modifications. As-synthesized iCONs demonstrated chemical stability and good antibacterial activity against both Gram-positive (*S. aureus*) and Gram-negative bacteria (*E. coli*). We speculate electrostatic interactions between positively charged iCONs and negatively charged phospholipid bilayer of bacterial membrane resulted in such antibacterial response. Taking into account these observations, we fabricated antibacterial $TpTG_{Cl}$@PSF membrane which could have potential medical benefits. Considering the water permeance and antibacterial property of this membrane, water purification process is currently underway in our laboratory.

ASSOCIATED CONTENT

Supporting Information

The Supporting Information is available free of charge on the ACS Publications website at DOI: 10.1021/jacs.5b13533.

Crystallographic data for $TpTG_{Cl}$ CIF)
Crystallographic data for TG_{Br} CIF)
Crystallographic data for TG_{Cl} monomer (CIF)
Synthesis and crystallographic details of ligand, molecular dynamics simulation study, biological experiments, membrane fabrication, characterization details (PDF)

AUTHOR INFORMATION

Corresponding Author

*r.banerjee@ncl.res.in

Author Contributions

$^{\nabla}$S.M, S.K, and B.P.B have contributed equally.

Notes

The authors declare no competing financial interest.

ACKNOWLEDGMENTS

R.B. acknowledges CSIR [CSC0122 and CSC0102], DST (SB/S1/IC-32/2013), DST Indo-Singapore Project (INT/SIN/P-05), and DST Nanomission Project (SR/NM/NS-1179/2012G) for funding. S.M. acknowledges CSIR Nehru Science PDF for financial help. S.K. acknowledges CSIR, and B.P.B. and A.K.M. acknowledge UGC for fellowship. We acknowledge Center for Advance Imaging, IIT Kanpur for AFM facility. We sincerely acknowledge Dr. T. G. Ajithkumar and Mr. Sanoop B. Nair for providing solid-state NMR facility, Dr. Guruswamy Kumaraswamy for PXRD facility, and Mr. Bikash Garai for SCXRD data acquisition.

REFERENCES

(1) (a) Berlanga, I.; Ruiz-Gonzalez, M. L.; Gonzalez-Calbet, J. M.; Fierro, J. L. G.; Mas-Balleste, R.; Zamora, F. *Small* **2011**, *7*, 1207−1211. (b) Berlanga, I.; Mas-Balleste, R.; Zamora, F. *Chem. Commun.* **2012**, *48*,

DOI: 10.1021/jacs.5b13533
J. Am. Chem. Soc. 2016, 138, 2823−2828

7976−7978. (c) Bunck, D. N.; Dichtel, W. R. *J. Am. Chem. Soc.* **2013**, *135*, 14952−14955. (d) Chandra, S.; Kandambeth, S.; Biswal, B. P.; Lukose, B.; Kunjir, S. M.; Chaudhary, M.; Babarao, R.; Heine, T.; Banerjee, R. *J. Am. Chem. Soc.* **2013**, *135*, 17853−17861. (e) Zhou, T.-Y.; Lin, F.; Li, Z. T.; Zhao, X. *Macromolecules* **2013**, *46*, 7745−7752. (f) Liu, X. H.; Mo, Y. P.; Yue, J. Y.; Zheng, Q. N.; Yan, H. J.; Wang, D.; Wan, L. − J. *Small* **2014**, *10*, 4934−4939. (g) Das, G.; Biswal, B. P.; Kandambeth, S.; Venkatesh, V.; Kaur, G.; Addicoat, M.; Heine, T.; Verma, S.; Banerjee, R. *Chem. Sci.* **2015**, *6*, 3931−3939. (h) Dong, R.; Pfeffermann, M.; Liang, H.; Zheng, Z.; Zhu, X.; Zhang, J.; Feng, X. *Angew. Chem., Int. Ed.* **2015**, *54*, 12058−12063. (i) Dong, W.-L.; Wang, L.; Ding, H.-M.; Zhao, L.; Wang, D.; Wang; Wan, C. L.-J. *Langmuir* **2015**, *31*, 11755−11759. (j) DeBlase, C. R.; Hernandez-Burgos, K.; Silberstein, K. E.; Rodriguez-Calero, G. G.; Bisbey, R. P.; Abruna, H. D.; Dichtel, W. R. *ACS Nano* **2015**, *9*, 3178−83. (k) Medina, D. D.; Rotter, J. M.; Hu, Y.; Dogru, M.; Werner, V.; Auras, F.; Markiewicz, J. T.; Knochel, P.; Bein, T. J. *J. Am. Chem. Soc.* **2015**, *137*, 1016−1019.

(2) (a) Zhang, Y.; Tan, M.; Li, H.; Zheng, Y.; Gao, S.; Zhang, H.; Ying, J. Y. *Chem. Commun.* **2011**, *47*, 7365−7367. (b) Wu, D.; Liu, R.; Pisula, W.; Feng, X.; Müllen, K. *Angew. Chem., Int. Ed.* **2011**, *50*, 2791−2794. (c) Liu, X.-H.; Guan, C. − Z.; Wang, D.; Wan, L.-J. *Adv. Mater.* **2014**, *26*, 6912−6920. (d) Gu, C.; Huang, N.; Gao, J.; Xu, F.; Xu, Y.; Jiang, D. *Angew. Chem., Int. Ed.* **2014**, *53*, 4850−4855. (e) Zhuang, X.; Mai, Y.; Wu, D.; Zhang, F.; Feng, X. *Adv. Mater.* **2015**, *27*, 403−427. (f) Cai, S.-L.; Zhang, W.-G.; Zuckermann, R. N.; Li, Z.-T.; Zhao, X.; Liu, Y. *Adv. Mater.* **2015**, *27*, 5762−5770. (g) Pfeffermann, M.; Dong, R.; Graf, R.; Zajaczkowski, W.; Gorelik, T.; Pisula, W.; Narita, A.; Müllen, K.; Feng, X. *J. Am. Chem. Soc.* **2015**, *137*, 14525−14532. (h) Liu, S.; Gordiichuk, P.; Wu, Z.-S.; Liu, Z.; Wei, W.; Wagner, M.; Mohamed-Noriega, N.; Wu, D.; Mai, Y.; Herrmann, A.; Müllen, K.; Feng, X. *Nat. Commun.* **2015**, *6*, 8817.

(3) (a) Côté, A. P.; Benin, A. I.; Ockwig, N. W.; Matzger, A. J.; O'Keeffe, M.; Yaghi, O. M. *Science* **2005**, *310*, 1166−1170. (b) Côté, A. P.; El-Kaderi, H. M.; Furukawa, H.; Hunt, J. R.; Yaghi, O. M. *J. Am. Chem. Soc.* **2007**, *129*, 12914−12915. (c) Wan, S.; Guo, J.; Kim, J.; Ihee, H.; Jiang, D. *Angew. Chem., Int. Ed.* **2008**, *47*, 8826−8830. (d) Wan, S.; Guo, J.; Kim, J.; Ihee, H.; Jiang, D. *Angew. Chem., Int. Ed.* **2009**, *48*, 5439−5442. (e) Spitler, E. L.; Dichtel, W. R. *Nat. Chem.* **2010**, *2*, 672−677. (f) Colson, J. W.; Dichtel, W. R. *Nat. Chem.* **2013**, *5*, 453−465. (g) Chen, X.; Addicoat, M.; Irle, S.; Nagai, A.; Jiang, D. *J. Am. Chem. Soc.* **2013**, *135*, 546−549. (h) Dalapati, S.; Jin, S.; Gao, J.; Xu, Y.; Nagai, A.; Jiang, D. *J. Am. Chem. Soc.* **2013**, *135*, 17310−17313. (i) Jin, S.; Supur, M.; Addicoat, M.; Furukawa, K.; Chen, L.; Nakamura, T.; Fukuzumi, S.; Irle, S.; Jiang, D. *J. Am. Chem. Soc.* **2015**, *137*, 7817−7827. (j) Xu, H.; Gao, J.; Jiang, D. *Nat. Chem.* **2015**, *7*, 905−912.

(4) (a) Kuhn, P.; Antonietti, M.; Thomas, A. *Angew. Chem., Int. Ed.* **2008**, *47*, 3450−3453. (b) Katekomol, P.; Roeser, J.; Bojdys, M.; Weber, J.; Thomas, A. *Chem. Mater.* **2013**, *25*, 1542−1548. (c) Hug, S.; Stegbauer, L.; Oh, H.; Hirscher, M.; Lotsch, B. V. *Chem. Mater.* **2015**, *27*, 8001−8010.

(5) Lanni, L. M.; Tilford, R. W.; Bharathy, M.; Lavigne, J. J. *J. Am. Chem. Soc.* **2011**, *133*, 13975−13983.

(6) Stegbauer, L.; Schwinghammer, K.; Lotsch, B. V. *Chem. Sci.* **2014**, *5*, 2789−2793.

(7) (a) Baek, K.; Yun, G.; Kim, Y. D.; Hota, R.; Hwang, I.; Xu, D.; Ko, Y. H.; Gu, G. H.; Suh, J. H.; Park, C. G.; Sung, B. J.; Kim, K. *J. Am. Chem. Soc.* **2013**, *135*, 6523−6528. (b) Payamyar, P.; Kaja, K.; Ruiz-Vergas, C.; Stemmer, A.; Murray, D. J.; Johnson, C. J.; King, B. T.; Schiffmann, F.; Vondele, J. V.; Renn, A.; Götzinger, S.; Ceroni, P.; Schütz, A.; Lee, L.-T.; Zheng, Z.; Sakamoto, J.; Schülter, A. D. *Adv. Mater.* **2014**, *26*, 2052−2058.

(8) (a) Budhathoki-Uprety, J.; Peng, L. L.; Melander, C.; Novak, B. M. *ACS Macro Lett.* **2012**, *1*, 370−374. (b) Qian, L.; Xiao, H.; Zhao, G.; He, B. *ACS Appl. Mater. Interfaces* **2011**, *3*, 1895−1901. (c) Yim, J. H.; Fleischman, M. S.; Rodriguez-Santiago, V.; Piehler, L. T.; Williams, A. A.; Leadore, J. L.; Pappas, D. D. *ACS Appl. Mater. Interfaces* **2013**, *5*, 11836−11843.

(9) Gong, Y. − H.; Miomandre, F.; Méallet-Renault, R.; Badré, S.; Galmiche, L.; Tang, J.; Audebert, P.; Clavier, G. *Eur. J. Org. Chem.* **2009**, *2009*, 6121−6128.

(10) (a) Müller, I. M.; Robson, R. *Angew. Chem., Int. Ed.* **2000**, *39*, 4357−4359. (b) Müller, I. M.; Möller, D.; Föcker, K. *Chem. - Eur. J.* **2005**, *11*, 3318−3324.

(11) (a) Desiraju, G. R.; Steiner, T. *The Weak Hydrogen Bond in Structural Chemistry and Biology*; Oxford University Press: Oxford, 2001. (b) Desiraju, G. R. *Acc. Chem. Res.* **2002**, *35*, 565−573.

(12) Kandambeth, S.; Mallick, A.; Lukose, B.; Mane, V. M.; Heine, T.; Banerjee, R. *J. Am. Chem. Soc.* **2012**, *134*, 19524−19527.

(13) Tabujew, I.; Freidel, C.; Krieg, B.; Helm, M.; Koynov, K.; Müllen, K.; Peneva, K. *Macromol. Rapid Commun.* **2014**, *35*, 1191−1197.

(14) (a) Li, P.; Sun, S.; Dong, A.; Hao, Y.; Shi, S.; Sun, Z.; Gao, G.; Chen, Y. *Appl. Surf. Sci.* **2015**, *355*, 446−452. (b) Bai, H.; Yuan, H.; Nie, C.; Wang, B.; Lv, F.; Liu, L.; Wang, S. *Angew. Chem., Int. Ed.* **2015**, *54*, 13208−13213.

(15) Yuan, Y.; Sun, F.; Zhang, F.; Ren, H.; Guo, M.; Cai, K.; Jing, X.; Gao, X.; Zhu, G. *Adv. Mater.* **2013**, *25*, 6619−6624.

(16) (a) Sasaki, D. Y.; Alam, T. M. *Chem. Mater.* **2000**, *12*, 1400−1407. (b) Salvio, R. *Chem. - Eur. J.* **2015**, *21*, 10960−10971.

(17) Yatvin, J.; Gao, J.; Locklin, J. *Chem. Commun.* **2014**, *50*, 9433−9442.

(18) (a) Kanehashi, S.; Masuda, R.; Yokoyama, K.; Kanamoto, T.; Nakashima, H.; Miyakoshi, T. *J. Appl. Polym. Sci.* **2015**, *132*, 42725. (b) Kozubek, A.; Tyman, J. H. P. *Chem. Rev.* **1999**, *99*, 1−25.

(19) Hu, W.; Peng, C.; Luo, W.; Lv, M.; Li, X.; Li; Huang, D. Q.; Fan, C. *ACS Nano* **2010**, *4*, 4317−4323.

DOI: 10.1021/jacs.5b13533
J. Am. Chem. Soc. 2016, 138, 2823−2828